Journal of Engg. Research ICAPIE Special Issue pp. 234-241 DOI:10.36909/jer.ICAPIE.15099

Synthesis and Electrochemical Performance of Acetylene Gas Decomposed Fe-Based Layered Oxide Cathode Material for Sodium-Ion Batteries

Abhishek Bhardwaj and A. K. Panwar*

*Corresponding Author: amrish.phy@dtu.ac.in

ABSTRACT

Sodium ion batteries (SIBs) surfacing into the market as one of the ordinate for electrical energy storage devices owing to plenty of raw material in nature and lower cost than well establish lithium ion battery technology. Therefore, the present study focuses on synthesis and electrochemical performance of the pristine NaFeO2 and C2H2 decomposed (carbon coated) NaFeO_2. A well crystallized, single phase O3-type α-NaFeO_2 was produced via solid-state method at 550 °C. X-ray diffraction patterns of the synthesized sample confirm the crystallinity and phase, followed by Rietveld refinement which confirms the Rhombohedral structure with R3 m space group. Particle morphology, distribution, shape and size were studied using SEM and the average crystallite size of 0.415 μm was obtained from Image J software. Energy Dispersive X-ray spectroscopy (EDS) proves the presence of Sodium and Iron are in the accordance to the stoichiometry of the synthesized compound. Electrochemical testing evident the more electrochemically stable and less resistive electrode is observed for carbon coated NaFeO_2.

Keywords: Sodium-Ion batteries; Cathode material; Carbon coating; NaFeO_2

INTRODUCTION

In recent years, the demand for advance and cheap energy storage system is very high due to their high usage in small portable devices to the heavy duty applications such as Grid energy storage, electric vehicles, aerospace applications, assets tracking systems, oil drilling and medical equipment. Presently, Li-ion batteries (LIBs) technology is the prime focus of the industry because of their better cyclability, high-energy and power densities, less self-discharge, and cheaper as compared to the other rechargeable batteries available in the market such as Ni-Cad and Ni-MH batteries (Song, Wang et al. 1999). On the other hand, safety, lifetime, poor low-temperature performance and cost are the major issues in the current lithium-ion batteries systems to be resolved. Therefore, in the quest to find an alternative to LIBs, Sodium-Ion batteries (SIBs) are being investigated as potential storage device for next-generation batteries.

SIBs have similar working principle as of LIBs. These are cost-effective alternative to the LIBs, particularly where battery's weight and energy density does not play any major roll for selection of the material like energy storage in grid form solar energy, wind, and other renewable energy sources. Moreover, SIBs also have good electrochemical properties such as high specific capacity, reversibility, and coulombic efficiency (Saadoune, Difi et al. 2014). Kikkawa et al. was the first to report α-NaFeO_2 to have sodium deintercalation in 1985 (Kikkawa, Miyazaki et al. 1985). Delams et. al has explained the classification of Rhombohedral α-NaFeO_2 as O3-type layered structure and Orthorhombic β-NaFeO_2 (Yabuuchi, Yoshida et al. 2012). β-NaFeO_2 does not show any electrochemical behaviour (Zhao, Zhao et al. 2013). Fascinatingly, Li+ and Fe3+ ions are similar in size, thus they are prone to cation mixing resulting counterpart of NaFeO_(2) while LiFeO_2 is known to be electrochemically inactive (Winter, Besenhard et al. 1998). Zhao Lee et al. has also reported the cathodic behaviour of NaFeO_(2) against Na anode (Zhao, Zhao et al. 2013). Upper cutoff voltage for 〖α-NaFeO〗_2 is limited to 3.4 V for good capacity retention. Theoretical capacity of NaFeO_2 is 241.8 mAh/g, supposing Fe3+/Fe4+ redox reaction to be topotactic one (Ohzuku and Ueda 1994).

In this study, the effect on the structural and electrochemical properties of the NaFeO_(2) and carbon coated NaFeO_2 via decomposition of acetylene gas as the carbon source has been investigated. For further notification NaFeO_(2)and cabon coated NaFeO_(2)is denoted as NFO and NFO/C. Hence, proper phase formation of NFO and NFO/C has been characterized with XRD. Particle shape, size and distribution is observed by SEM. Elemental analysis and electronic conductivities of synthesized materials has been carried out using EDX and source meter, respectively. Electrochemical measurement has also been reported for both the NFO and NFO/C in terms of EIS and CV.

EXPERIMENTAL

MATERIAL SYNTHESIS

Stoichiometric amounts of the sodium peroxide (Na_2 O_2) and Iron(III) oxide (Fe_2 O_3) (all of precursors are of Sigma Aldrich, grade ≥ 99%) were wet-milled using Retsch make planetary ball mill (PM 100) with stainless steel (SS) vessel. The precursors were effectively milled for 6 hours in ethanol media at 450 rpm keeping the ball to powder ratio 10:1. After ball milling, the resulting homogenous powder was ground to fine powder using pestle mortar. This grounded fine powder was calcined at 550°C for 12 hours in a tubular furnace. The synthesized material is taken out at 550 °C from the furnace and without cooling transferred instantly to Argon filled Glove Box make mbraun and kept inside to avoid further oxidation. Furthermore, for carbon coated sample, as prepared NFO was heated at 700 °C in a slightly reducing atmosphere ($Ar : H_2$ :: 95 : 5 vol%) and then C_2 H_2 gas is passed for 20 minutes to obtain NFO/C. The flow rate of all three gases: Ar, H_2 and C_2 H_2 inside tubular furnace was kept 200 sccm, 10 sccm and 50 sccm, respectively. The constant flow of these gases were maintained by Alicat scientific make mass flow controllers.

MATERIAL CHARACTERIZATION

Thermogravimetric analysis (TGA) and differential thermal analysis (DTA) has been performed under oxygen atmosphere using Perkin Elmer make TGA 4000 system. Ball milled powdered sample was heated at the rate 10°C/min till the temperature reaches up to 900 °C. Phase formation of NFO and NFO/C was examined from the XRD patterns obtained using Rikagu make Ultima-IV, X-ray diffractometer with CuKα1 radiation of the wavelength, 1.540 Å. Wide range XRD patterns were scanned in the range of 100 – 800 with the step size of 0.020. Micro-structural analysis of the specimen was performed by Zeiss made SEM with attached EDX. Measurement of resistivity has been carried out with change in temperature from room temperature to 275°C using Keithly make 6430 Sub-Femtoamp Remote Source Meter.

ELECTRODE PREPARATION AND ELECTROCHEMICAL CHARACTERIZATION

For electrochemical reversibility of NFO and NFO/C electrodes for half coin-cells (CR2032) were fabricated inside the Ar filled glove box attaining O_2/ H_2 O levels < 0.5 ppm. The working electrode of the two samples were composed by dispersing NaFeO_(2), super P (conductive carbon) polyvinylidene difluoride (PVDF as binder) in the ratios of 80:10:10 wt% in N-methyl-2-pyrrolidinone (NMP). In order to make it homogenous, mixture of all three ingedients was stirred under vacuum for 4 hrs and then pasted uniformly over Al foil current collector and dried at 120 °C using Gelon make automatic coating unit. Circular electrode disc of diameter 16 mm was punched and effective mass loading was found to be ~2 mg. The electrode was then again dried in a vacuum oven at 60°C for 2 hrs before transferring it to glove box. Pure metallic sodium was used as reference electrode. For electrolyte, NaClO_4 dissolved in solvents EC and DEC in the ratio of 1:1 vol%. A glass-fibre filter(GB-100R) has been used as a separator. Electrochemical impedance spectroscopy (EIS) data is measeured in the frequency range of 100 kHz- 10 mHz in an AC voltage pulse of 5mV, cyclic voltammetry (CV) results were observed over the voltage range of 2.5-3.6 V (versus Na/Na+ metal). All the electrochemical tests were performed at 298.15 K using Biologic make potentiostat-VMP3 model.

RESULTS AND DISCUSSION

THERMOGRIVEMETRIC STUDY (TGA-DTA)

TGA-DTA results are observed and shown in Figure 1. It was observed that the mass of the sample was reduced at three different stages. Stage-1 represents the weight loss of 8.27% at the temperature range of 30-105°C, at this stage moisture absorbed by the sample evaporates. Stage-II and stage-III indicates the weight loss of 10.47 % and 8.12% depicting the formation of NaFeO_2 occurs in two stages. DTA is in accordance to TGA, showing endothermic dip where TGA shows mass loss stages.

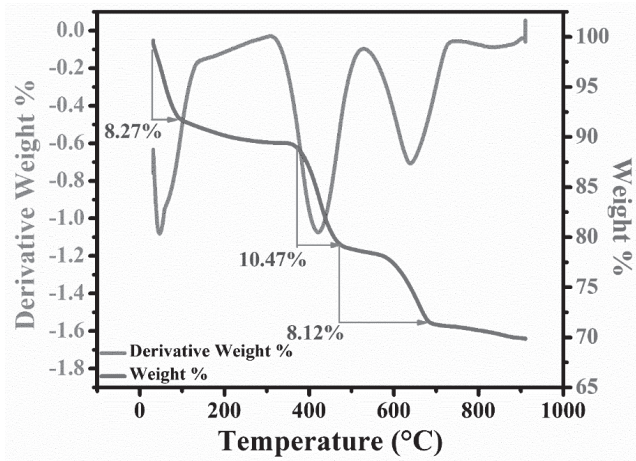

Figure 1 . TGA-DTA curve for NaFeO2 under O2 atmospheres.

STRUCTURAL ANALYSIS

Figure 2(a) and (b) indicate the XRD patterns of synthesized NFO, NFO/C and the Rietveld refined results of NFO samples. Figure 2 (c) shows schematic structure for the NFO sample. The Na and Fe ions are octahedrally aligned with the O atoms (Li, Gao et al. 2018). X-Ray Diffractogram of the as synthesized NFO (NaFeO_2) is in accordance with α-NaFeO_2 (ICSD: 01-082-1495). Diffractogram shows no impure crystallinity. These synthesized samples were indexed to Rhombohedral structure with R-3m space group. Peaks of the XRD patterns are sharp and intense,

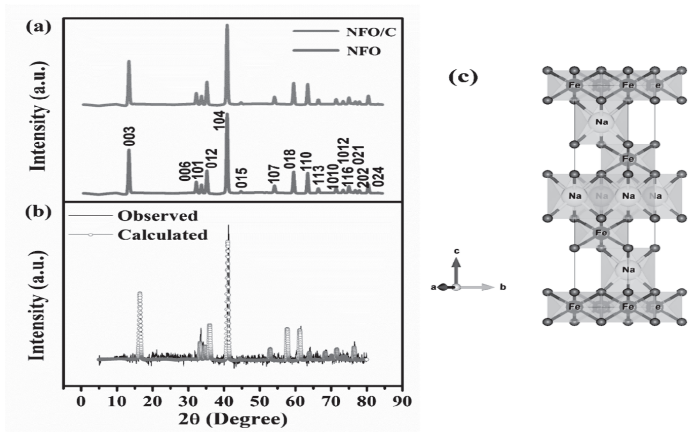

Figure 2 . (a) XRD pattern of as obtained NFO and NFO/C, (b) Rietveld Refinement of NFO (C) Schematic Structure of NFO

depicting proper crystallinity. Rietveld refinement confirms the structure and used to estimate the refined lattice parameters.

The lattice constant obtained after refinement and phase matching with standard ICSD card are shown in Table 1.

Table 1. The unit cell parameters for ICSD and Obtained Product.

Sample / Database file	a (Å)	b (Å)	c (Å)
ICSD card:01-82-1495	3.022	3.022	16.081
NFO	3.019 (5)	3.019 (5)	16.069 (5)

The small value Rwp/% (=3.17) indicates that the fitted profile is in the acceptable range. When cation atomic occupancy is kept lower then 1, best fitting results were obtained. The obtained Rietveld refinement results were tabulated below in Table 2.

Table 2. Crystal Structure Parameters of NFO, obtained from Rietveld Refinement

Atom	Wyckoff	x	y	Z	Occupancy	B_{eq}
Na	3a	0.0	0.0	0.5	1.0	0.5
Fe	3b	0.0	0.0	0.0	1.0	0.5
O	6c	0.0	0.0	0.266	1.0	0.5

SEM-EDX STUDY

Figure 3(a) and (b) displays SEM micrographs of NFO and NFO/C with EDX results having weight% of all the elements in the inset. These graphs reveals that NFO have nearly spherical.

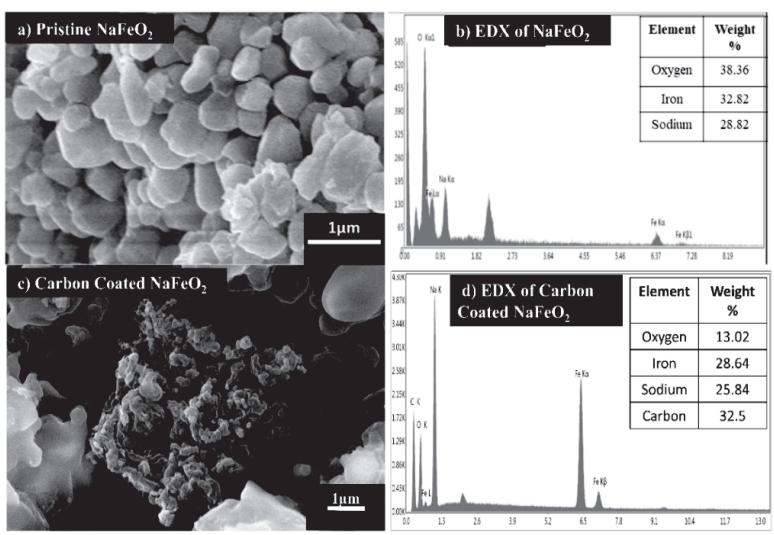

Figure 3. SEM micrograph of as synthesized (a) NFO, (c) NFO/C and EDX graph of (b) NFO and (d) NFO/C

shape with average diameter of 368 μm and fairly narrow particle distribution range.

RESISTIVITY WITH RESPECT TO TEMPERATURE

Figure 4 depicts resistivity vs temperature graphs for pristine NFO and NFO/C synthesized using solid state reaction route. It was observed that resistivity of the pristine NFO and NFO/C decreases with an increase in temperature from 5.9 x 10^8 (Ω.mm) to 1.6 x 10^7 (Ω.mm) and 5.9 x 10^9 (Ω.mm) to 4.6 x 10^6 (Ω.mm) respectively on increasing temperature from room temperature i.e. 38 °C to 200 °C, respectively.

$$\sigma = {}^{1}/_{\rho} \tag{1}$$

Electronic conductivity (σ) is the reciprocal of the electrical resistivity (ϱ). Therefore, Conductivity of the NFO and NFO/C at room temperature is 0.18 x $10^{(-9)}$ S $cm^{(-1)}$ and 3.57 x $10^{(-9)}$ S cm(-1). Arrhenius equation was used to calculate Activation energy (E_a):

$$\sigma = \sigma_0 \exp\left(\frac{-E_a}{K_b T}\right) \tag{2}$$

where σ is electronic conductivity (S $cm^{(-1)}$), K_b stands for Boltzmann constant (J $K^{(-1)}$), and T

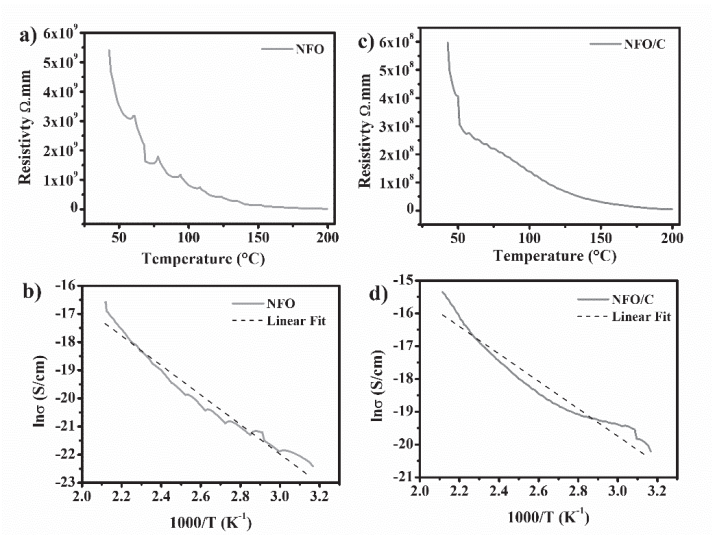

Figure 4. Resistivity of (a) NFO and (b) NFO/C samples with respect to change in temperature and figure 4 (c) & (d) displays variation in DC electric conductivity σ with temperature range of 38 °C to 200 °C

stands for temperature (K). Activation energy of the NFO and NFO/C were found to be 43.62 meV and 34.70 meV respectively. Decrease in activation energy is mainly due to high ionic conductive nature of carbon coating.

ELECTROCHEMICAL STUDY

CYCLIC VOLTAMMETRY (CV) AND ELECTROCHEMICAL IMPEDANCE SPECTROSCOPY(EIS)

Figure 5(a) and (b) displays the cyclic voltammogram of NFO and NFO/C samples recorded at the 0.05 mV $s^{(-1)}$ scan rate versus Na^+/Na at room-temperature(RT). Both samples show similar CV curves. Potential difference of the anodic peaks for 1st two cycles for NFO/C (0.03 V) is much smaller than for NFO (0.05V). This trend is also followed by cathodic peaks, for NFO/C (0.01V) and NFO (0.06V). Current intensity for both the cycles of NFO and NFO/C also shows similar results, indicating increase in the redox stability for NFO/C in comparison to the bare NFO. From the anodic and cathodic peaks of both the samples it can also be observed that intensity ratio $\left(\frac{I_A}{I_C}\right)$ reduces from 1.8 to 1.5

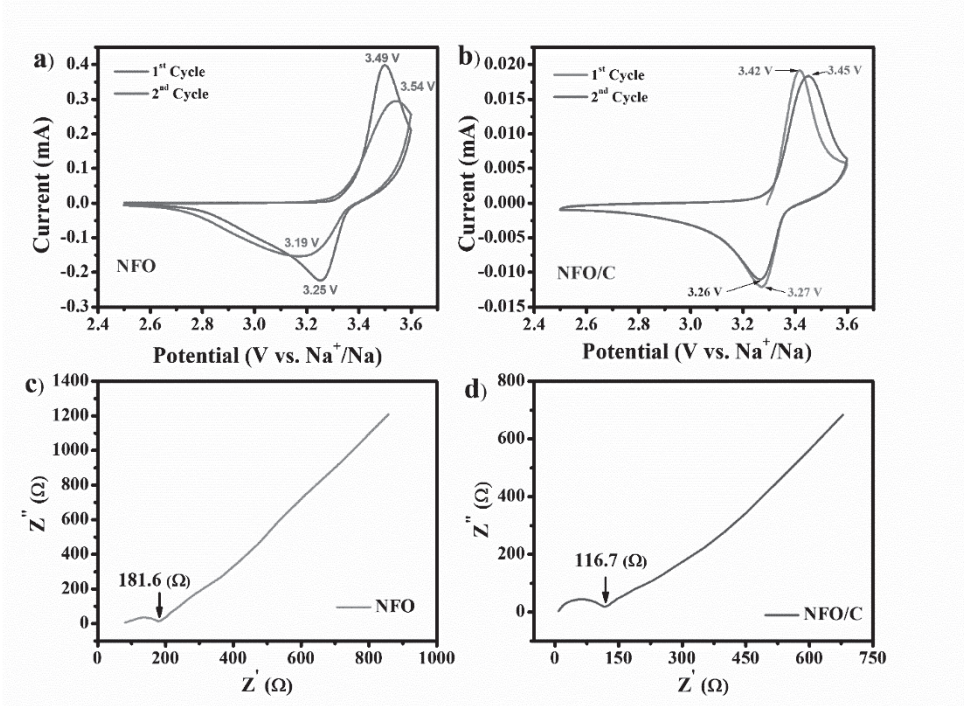

Figure 5. Cyclic voltammetry curves of (a) NFO and (b) NFO/C samples and and EIS curves of (c) NFO and (d) NFO/C samples

for carbon coated samples this implies increase in reversibility of Na^+ ion. Figure 5(c) and (d) displays the EIS curves observed for both the samples under the frequency interval of 100 kHz - 10 mHz using 5 mV amplitude voltage pulse. It can be observed that at high frequency region EIS curves displays the semi-circular graph along with a straight line at lower frequency region. From the intercept of the semi-circle, ohmic-resistance (R_s) of the cell has been calculated, which depicts the resistance of the electrode and electrolyte interface. Sodium ion diffusion coefficient in the bulk electrode has been determined by the Warburg impedance (Z_w) associated with the straight line present in the low frequency region. Sodium ion diffusion was calculated using the following formula:

$$D = \frac{R^2T^2}{2A^2n^4F^4C^2\sigma_W^2} \quad (3)$$

Here, D, A, σw, n, C, T, F and R are the sodium-ion diffusion coefficient (cm2 s-1), electrode area (cm-2), Warburg factor, number of electrons involved in the redox reaction (in our case 1), sodium-ion concentration (~ 10^{-3} mol cm^{-3}), absolute temperature (K), faraday constant (96486 C mol-1), and gas constant (8.314 J mol-1 K^{-1}), respectively, which is related to Z' by the following reaction (Saroha and Panwar 2017):

$$Z' = R_s + R_{ct} + \sigma_w \omega^{-0.5} \quad (4)$$

Calculation of the Warburg impedance coefficient was done using the equation (4) and substituted in equation (3), to obtain the sodium-ion diffusion coefficients of the NFO and NFO/C samples. Figure 6 depicts the relationship between Z' and $\omega^{(-0.5)}$. The sodium ion diffusion coefficients (D) of the NFO and NFO/C samples are shown in the table 3.

Table 3. Electrochemical Impedance results for NFO and NFO/C samples

Sample	R_{ct} (Ω)	σ_w (Ω $s^{-0.5}$)	D ($cm^2 s^{-1}$)
NFO	181.6	134.43	4.85 x 10^{-13}
NFO/C	116.7	219.55	1.81 x 10^{-13}

From the table 3, it is clearly visible that carbon coated NaFeO_2 has lower charge transfer resistance and higher diffusion coefficient.

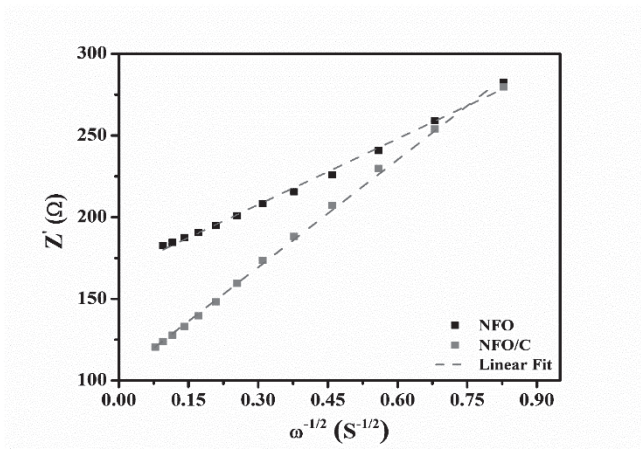

Figure 6. Curve between Z' and $\omega^{(-0.5)}$ in low frequency region.

CONCLUSION

In this study, carbon coating NaFeO_2 were synthesized using decomposition of Acetylene gas. XRD confirms the formation of well crystalline rhombohedral phase. No additional impurity phase was found in the sample. SEM studies depicts nearly spherical shaped, to some extent agglomerated particles. Electrical resistivity studies depict the carbon coated samples to be more conductive than the bare sample. Electrochemical studies such was CV and EIS reveal that carbon coated NaFeO_2 is much better electrode in comparison to the bare NaFeO_2. CV curve depicting nearly retractable first two cyclic curves for carbon coated NaFeO_2 whereas EIS curves reveals carbon coated $NaFeO_2$ to have lower impedance value.

ACKNOWLEDGMENT

The authors gratefully acknowledge Delhi Technological University financial support (reference No.: F. No. DTU/IRD/619/2019/2114) to carry out this research work under the project grand.

REFERENCES

Kikkawa, S., et al. (1985). "Sodium deintercalation from α-NaFeO2." Materials Research Bulletin 20(4): 373-377.

Li, Y., et al. (2018). "Iron migration and oxygen oxidation during sodium extraction from NaFeO2." Nano energy 47: 519-526.

Ohzuku, T. and A. Ueda (1994). "Why transition metal (di) oxides are the most attractive materials for batteries." Solid State Ionics 69(3-4): 201-211.

Saadoune, I., et al. (2014). Electrode materials for sodium ion batteries: A cheaper solution for the energy storage. Optimization of Electrical and Electronic Equipment (OPTIM), 2014 International Conference on, IEEE.

Saroha, R. and A. K. Panwar (2017). "Effect of in situ pyrolysis of acetylene (C2H2) gas as a carbon source on the electrochemical performance of LiFePO4 for rechargeable lithium-ion batteries." Journal of Physics D: Applied Physics 50(25): 255501.

Song, J., et al. (1999). "Review of gel-type polymer electrolytes for lithium-ion batteries." Journal of Power Sources 77(2): 183-197.

Winter, M., et al. (1998). "Insertion electrode materials for rechargeable lithium batteries." Advanced Materials 10(10): 725-763.

Yabuuchi, N., et al. (2012). "Crystal structures and electrode performance of alpha-NaFeO2 for rechargeable sodium batteries." Electrochemistry 80(10): 716-719.

Zhao, J., et al. (2013). "Electrochemical and thermal properties of α-NaFeO2 cathode for Na-ion batteries." Journal of The Electrochemical Society 160(5): A3077.

Zhao, J., et al. (2013). "Electrochemical and thermal properties of α-NaFeO2 cathode for Na-ion batteries." Journal of The Electrochemical Society 160(5): A3077-A3081.